Pore geometry of Permo-Triassic sandstone from measurements of electrical spectroscopy

JULIAN B. T. SCOTT & R. D. BARKER

School of Geography, Earth and Environmental Sciences, University of Birmingham, Birmingham B15 2TT, UK

Abstract: In order to provide an indirect method of estimating the hydraulic properties of sandstone aquifer rocks, electrical spectroscopy measurements were made on Permo-Triassic Sandstone over the frequency range 0.0001–1000 Hz. Samples from several boreholes across Britain are shown to exhibit a phenomenon called electrical relaxation, which we have modelled using a generalized Cole–Cole equation. The Cole–Cole parameters correlate well with other hydrogeologically important parameters determined using mercury injection capillary pressure and nitrogen adsorption techniques. Of greatest importance is that the relaxation time, τ, is strongly related to the dominant pore-throat size from which intergranular permeability may be estimated. A normalized version of the chargeability appears to be related to the surface conductivity and this gives the possibility of estimating the pore surface area to volume ratio, a value that is important in determining both permeability and sorption. The potential uses of electrical spectroscopy in hydrogeology and many other fields, including geology and petroleum petrophysics, are only now becoming apparent, and further advances are certain.

Low-frequency electrical spectroscopy is the measurement and analysis of the variation of electrical resistivity with frequency of the applied current. In geophysics it is often called spectral induced polarization (SIP) and has been used for many years, mainly for mineral resource location and discrimination (Van Voorhis *et al.* 1973; Pelton *et al.* 1978). Work over the last 20 years has shown that electrical spectroscopy can also provide useful information on non-mineralized sedimentary rocks and soils, from characterization of internal structure to determination of pore-fluid chemistry and contamination (Olhoeft 1985; Börner *et al.* 1993; Slater & Lesmes 2002). However, in the past, the variation in properties over the lowest frequency range 0.0001–1000 Hz has often been ignored due to either limited measurement capability or because studies focused on rock types with little frequency variation, but it is in this frequency range where the most interesting and useful information is now being obtained (Lesmes & Morgan 2001; Scott & Barker 2003).

The Permo-Triassic sandstone is the second most important aquifer in England and Wales, providing much of the groundwater abstraction for major conurbations including Birmingham and Manchester (Allen *et al.* 1997). A knowledge of its small-scale internal structure and hydraulic properties is important in understanding fluid flow through the sandstone and in water resource and contaminant studies. It is possible that this information may be obtained indirectly from measurements of spectral induced polarization. Here we present the first detailed study of spectral induced polarization of Permo-Triassic sandstone from the British Isles. The results are compared with hydrogeologically important parameters, such as cation-exchange capacity, pore surface area and pore-throat size distributions, determined using a variety of other techniques. We provide details of the measurements and develop some explanations for the observations.

Electrical spectroscopy

Conventional measurement of resistivity is achieved by passing a direct electrical current through a material while monitoring the voltage. The resistance is computed from the ratio of the voltage to current, and the material property, i.e. its resistivity, is determined by multiplying the resistance by some factor that accounts for the size of the sample and the geometry of the measuring contact points (electrodes).

When an alternating current is employed, the observed voltage will often be slightly out of phase with the applied current. The phase shift (φ) as well as the resistivity magnitude (ρ) are normally measured. These quantities generally vary with frequency of the applied current and

From: BARKER, R. D. & TELLAM, J. H. (eds) 2006. *Fluid Flow and Solute Movement in Sandstones: The Onshore UK Permo-Triassic Red Bed Sequence.* Geological Society, London, Special Publications, **263**, 65–81.
0305-8719/06/$15

are therefore measured at a number of different frequencies, hence the term electrical spectroscopy. Often the in-phase (real) and out-of-phase (quadrature) components of resistivity (ρ', ρ'') or conductivity (σ', σ'') are used and these can be related to the phase shift φ by

$$\tan \varphi = \frac{\rho''}{\rho'} = -\frac{\sigma''}{\sigma'} \quad (1)$$

and the resistivity and conductivity magnitudes (ρ^* and σ^*) by

$$\rho^* = \sqrt{\rho'^2 + \rho''^2} \text{ and } \sigma^* = \sqrt{\sigma'^2 + \sigma''^2}. \quad (2)$$

The complex resistivity and conductivity are related to each other and to the dielectric permittivity (ε^*) by

$$\sigma^* = \frac{1}{\rho^*} = i\omega\varepsilon^*, \text{ where } i = \sqrt{-1}. \quad (3)$$

The frequency-dependent phase shift is the result of a phenomenon known as polarization, which is caused by a relative shift of positive and negative charges (Jonscher 1983, 1996). Going from small to large scale, some of the main polarization causes are the shifting of electric fields around individual atoms, the realignment of dipolar molecules and ionic diffusion. These different processes act at different speeds when an electric field is applied. It takes a finite time (the relaxation time) after the application of an electric field for the charges to realign or redistribute themselves and the same length of time to return to equilibrium after cessation of that field. When an alternating sinusoidal field is applied with a period much longer than a particular relaxation time, that process will seem to happen almost instantaneously and not contribute to the out-of-phase (quadrature) response. When the period is much shorter than the relaxation time, there will be no significant charge movement and therefore no contribution to the quadrature response. When the period is the same as the relaxation time there will be a maximum quadrature response.

Electrical spectroscopy is used for a wide range of scientific applications. These include investigating the physics of liquids and monitoring biological systems. Complex electrical measurements for these and other purposes are regularly made over the frequency range of 10^{-6}–10^{12} Hz (Kremer 2002). Electrical relaxation phenomena are very important in electrical spectroscopy, occurring in many different materials at all frequencies, and have a wide variety of causes, although these are often poorly understood.

The aim of the work presented here is an analysis of the polarization response observed in the Permo-Triassic sandstone over relatively low frequencies (0.0001–1000 Hz), below the point at which inductive charge transfer becomes significant.

Laboratory measurements on Permo-Triassic sandstone

Sandstone samples

Twenty-eight samples of Permo-Triassic sandstone were taken from eight boreholes distributed across the sandstone outcrop in England (Fig. 1), the exception being the Winterbourne Kingston samples which were obtained from a deep oil exploration borehole. The samples were chosen to provide a wide variety of sandstone types from within the UK Permo-Triassic. Their petrological characteristics, determined from thin section and optical and scanning electron microscope studies, are summarized in Table 1. In addition all sandstones had a small percentage of iron oxide and clay (illite–smectite) coating the grains.

Electrical measurements

For the electrical measurements, all samples were cut into cylindrical cores each measuring

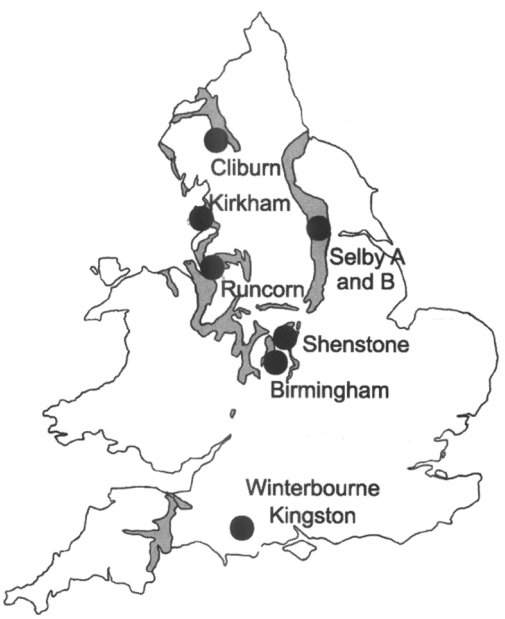

Fig. 1. Map of the boreholes sampled in this study. The main Permo-Triassic sandstone areas of England and Wales are shaded grey.

Table 1. *Sandstone sample descriptions*

Site	Samples	Formation	Description
Birmingham	Ba4, Ba10-12, Ba18, Ba21, Ba23, Ba31, Ba33, Ba34A/B, Ba37, Ba40, Ba42	Wildmoor	Variable, red-brown soft, poorly-cemented, sublitharenitic sandstone (B40 bleached grey, B18 contains 1 mm thin marl parting)
Cliburn	C7, C8	Penrith Sandstone	Dark red, fluvial sandstone with some feldspar
Kirkham	K7, K9, K10	Helsby Sandstone	Coarse-grained, well-sorted, aeolian sandstones with quartz overgrowths (K7 fluvial)
Runcorn	R5, R7, R16, R18	Helsby Sandstone	Coarse-grained, aeolian, arkosic sandstones
Selby A	Sa7	Wildmoor	Red, poorly-cemented fluvial sandstone
Selby B	Sb3	Wildmoor	Red, poorly-cemented fluvial sandstone
Shenstone	SH4	Kidderminster	Poorly-sorted, red, medium- to coarse-grained litharenite
Winterbourne Kingston	W2, W9	Otter Sandstone	Fine to coarse, pale red sandstones with up to 30% feldspar, carbonate (largely dolomite) cement, much unconnected pore space

35 mm in diameter and 30–70 mm in length. The samples were dried at 80 °C for 48 h. Tests confirmed that electrical results were the same as when samples are dried at lower temperatures for longer times (Scott *et al.* 2003). The samples were then vacuum saturated with a synthetic groundwater containing 60 mg l^{-1} Ca^{2+}, 30 mg l^{-1} Mg^{2+}, 34 mg l^{-1} Na^{+}, 142 mg l^{-1} Cl^{-}, 120 mg l^{-1} SO_4^{2-} and 30 mg l^{-1} HCO_3^{-}, a chemistry that closely matched the cation concentrations in the Triassic sandstone aquifer measured at the University of Birmingham borehole (Mitchener 2003). The same water was used for all the samples, irrespective of origin, in order to provide a firm basis for comparison. The measured synthetic groundwater resistivity varied slightly between samples, from 11.5 to 14 Ωm, due to difficulty in accurate reproduction of the ionic balance.

Measurements of the resistivity magnitude and the phase angle were made at several frequencies over the range of 10^{-3}–10^{3} Hz, using a SIP–Fuchs spectral IP system, a commercially available system from Radic Research. This passes a sinusoidal current through the sample at set frequencies, starting at 1500 Hz, then decreasing in steps of a half down to 1.43 mHz, giving a total of 21 readings. Lower frequencies were needed for the measurement of sample Ba12, in order to fully characterize its phase spectrum, and this was done using a standard impedance analyser and software specifically written for this purpose at the Department of Electrical Engineering, University of Birmingham.

Over this low-frequency range it is important to use a four-electrode measurement technique and for this the sample cell of Taylor & Barker (2002) was used along with Ag–AgCl non-polarizing electrodes. The measurement temperature, was the ambient laboratory temperature which was monitored to ensure stability at 20 ± 1 °C. Errors due to the experimental system were checked by repeating measurements for a number of samples on a system using circular potential electrodes at the Technical University of Clausthal (TUC), Germany (Scott *et al.* 2003; no significant differences were found.

The electrical results are presented in the form of resistivity and phase spectra. The phase shift is normally negative and so is conventionally plotted with the negative phase scale up. In this way the phase spectra generally show a relaxation 'peak' (Fig. 2), which appears at different frequencies for different samples and occurs over the range of 10^{-4}–10 Hz. This demonstrates that different relaxation times are dominant for different samples. In order to determine the dominant relaxation times and other important induced polarization parameters, the data were modelled using the generalized Cole–Cole equation (Klein & Sill 1982; Dias 2000):

$$\rho^* = \rho_0\left[1 - m\left(1 - \frac{1}{[1+(i\omega\tau)^c]^k}\right)\right] \qquad (4)$$

where $0 \le (c;k) \le 1$, ρ^* is the complex resistivity and ρ_0 is the resistivity at the limit as ω tends to 0. The parameter, m, gives the magnitude of

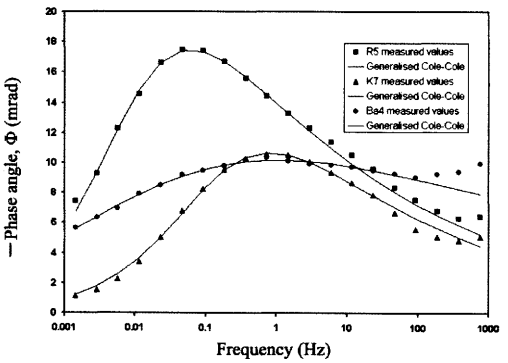

Fig. 2. Electrical phase-angle spectra with generalized Cole–Cole model parameter fitting at frequencies of less than 100 Hz.

the polarization and is roughly equivalent to the chargeability as defined by Seigel (1959). The model parameters c and k give the symmetrical and asymmetrical distribution of relaxation times around a central relaxation time of τ.

The model fitting was carried out for at least 12 data points around the phase peak region using a least-squares minimization routine. Points at frequencies over 100 Hz were not included in the fitting process in order to avoid any influence of electromagnetic coupling across the sample, the effects of which start to appear at higher frequencies. In all cases it was possible to obtain a fit to within experimental error, although with spectra that had low phase angles or a widely spread relaxation peak a wider range of parameters could provide a good fit to the spectra. For this reason the model fitting was repeated several times to find the range of each parameter that could give a good fit to the data. The mean value for each parameter is given in Table 2, along with the range of values fitted and the parameter errors. For the low-frequency resistivity, ρ_0, the value used was the resistivity at 5 mHz ($\rho_{5\,\mathrm{mHz}}$), chosen to avoid the occasional measurement errors occurring at very low frequencies and which were due to the long duration of individual measurements. The generalized Cole–Cole model fits to three of the samples (Fig. 2) demonstrate how well the asymmetric data can be modelled. The slight increase in phase angle above 100 Hz is largely due to electromagnetic coupling across the sample holder and is therefore not a property of the sandstone and so was not included in the modelling.

The chargeability, m, determined from the generalized Cole–Cole modelling, is a measure of the polarization. However, the magnitude of m will also depend on the in-phase conductivity of the bulk pore fluid. In order to isolate the effects of the pore surface it is necessary to normalize m by dividing it by the in-phase resistivity (Lesmes & Frye 2001), so that

$$m_n = m\sigma_0 = \frac{m}{\rho_0}. \quad (5)$$

This normalized chargeability m_n can also be compared to σ'', which is considered to be closely linked to the surface conduction in the rock matrix (Vinegar & Waxman 1984).

Cation-exchange capacity (CEC)

CEC is a measure of the ability of the rock to exchange cations between the pore surface and the saturating solution. As exchange sites occur mainly on pore-lining clays and oxyhydroxides, the CEC is one measure of the quantity of pore-lining material present in the rock. The standard way to measure CEC is to saturate the exchange sites with a cation that preferentially bonds to these sites and does not occur in the groundwater chemistry. The method used was first to disaggregate the rock with a pestle and mortar, and then saturate it with ammonium chloride, in order to replace all the cation-exchange sites with ammonium ions. The released cations in solution are then detected using ICP-AES (inductively coupled plasma-atomic emission spectrophotometry) and the CEC of the rock determined. A correction is made for the increase in carbonate due to some cations being released along with the carbonate cement and not coming from the exchange sites, by using a standard carbonate alkalinity titration. Rather than use the CEC in petrophysical applications, it is more common to use the cation exchange to pore volume ratio (Q_v) (Vinegar & Waxman 1984; Sen *et al.* 1990) given by

$$Q_v = \frac{1}{100} \times \mathrm{CEC}\left[\frac{1-\phi}{\phi}\right] d_m \quad (6)$$

where ϕ is the fractional porosity, d_m is the matrix density in g cm^{-3}, CEC is in meq 100 g^{-1} and Q_v is in units of meq ml^{-1}.

Surface area analysis

Surface area analysis is commonly carried out using the nitrogen adsorption method. This has an advantage over mercury injection in that it is not affected by bottleneck pores (Lowell & Shields 1991) that occur in sandstones and could

Table 2. *Generalized Cole–Cole parameters for Permo-Triassic sandstone samples*

Sample	$\rho_{5\ mHz}$ (Ωm) error = 2%	m	± m error	τ (s)	τ error (s)	c	± c error	k	± k error	m_n (S m^{-1})	Frequency range fitted (Hz)
Ba4	98.9	0.159	0.013	25	10	0.35	0.03	0.20	0.05	0.00161	0.001–100
Ba10	73.7	0.071	0.010	17	6	0.72	0.05	0.20	0.07	0.000963	0.001–3
Ba11	86.3	0.070	0.001	35	25	0.24	0.04	0.91	0.09	0.000811	0.001–3
Ba12	90.8	0.153	0.001	335	10	0.35	0.01	0.99	0.02	0.00169	0.0003–0.3
Ba18	51.9	0.088	0.002	37	7	0.57	0.04	0.38	0.06	0.00170	0.001–3
Ba21	32.0	0.148	0.066	1.4	0.8	0.37	0.04	0.15	0.08	0.00463	0.04–100
Ba23	78.4	0.088	0.005	18	4	0.59	0.04	0.21	0.02	0.00170	0.001–3
Ba31	62.0	0.074	0.001	4.7	0	0.58	0.00	0.61	0.00	0.00119	0.001–3
Ba33	50.6	0.067	0.001	3.3	0.3	0.61	0.01	0.33	0.02	0.00132	0.002–11
Ba34A	53.0	0.094	0.003	2.8	0.2	0.64	0.02	0.30	0.03	0.00177	0.005–50
Ba34B	60.4	0.084	0.002	2.8	0.4	0.58	0.02	0.35	0.04	0.00139	0.005–50
Ba37	64.9	0.075	0.001	3.8	2.4	0.58	0.01	0.34	0.03	0.00116	0.005–11
Ba40	37.0	0.093	0.001	1.4	0.1	0.53	0.01	0.29	0.02	0.00251	0.01–100
Ba42	78.7	0.061	0.003	14	2	0.65	0.08	0.17	0.04	0.000775	0.01–100
C7	88.0	0.091	0.002	11	1	0.65	0.02	0.35	0.03	0.00103	0.001–3
C8	74.6	0.145	0.002	11	1	0.57	0.02	0.37	0.03	0.00194	0.001–6
K7	88.8	0.074	0.001	1.4	0.2	0.61	0.01	0.29	0.01	0.000833	0.01–100
K9	213	0.057	0.003	33	22	0.30	0.03	0.29	0.03	0.000268	0.001–3
K10	217	0.058	0.002	50	30	0.29	0.02	0.53	0.12	0.000267	0.001–3
R5	99.5	0.102	0.002	19	2	0.70	0.03	0.26	0.03	0.00103	0.001–3
R7	106	0.130	0.002	18	3	0.51	0.02	0.35	0.04	0.00123	0.002–25
R16	69.0	0.125	0.003	6.9	1.5	0.62	0.04	0.27	0.02	0.00181	0.002–100
R18	83.5	0.115	0.007	21	0	0.58	0.03	0.32	0.01	0.00138	0.001–12
Sa7	32.8	0.097	0.007	0.74	0.37	0.42	0.02	0.56	0.07	0.00296	0.01–100
Sb3	49.2	0.111	0.011	11	1	0.63	0.04	0.25	0.02	0.00226	0.01–6
SH4	152	0.119	0.002	15	5	0.37	0.02	0.57	0.08	0.000743	0.001–3
W2	127	0.041	0.019	9.8	5.2	0.56	0.06	0.06	0.04	0.000323	0.002–25
W9	109	0.044	0.003	33	28	0.27	0.08	0.35	0.20	0.000404	0.002–25
Max.	217	0.153		335		0.72		0.99		0.00463	
Min.	32.0	0.041		0.74		0.24		0.06		0.000267	
Mean	87	0.09		27		0.5		0.4		0.00141	
SD	46	0.03		62		0.1		0.2		0.00091	

give artificially high values for surface area. Surface area is fractal in nature and the smaller the unit of area the measurement tool is capable of measuring, the larger the value of surface area obtained. Nitrogen adsorption measures pore space down to the scale of the size of a nitrogen molecule (about 3.5 Å) and is therefore capable of measuring much of the surface roughness provided by the pore-lining material. There are several methods for calculating the surface area from nitrogen adsorption, the most common method being the Brunauer, Emmett and Teller (BET) method (Lowell & Shields 1991).

Nitrogen adsorption was carried out using the Micromeritics ASAP 2010 chemisorption equipment. Samples used for nitrogen adsorption analysis were taken from the end cuts of the cylindrical samples used for the electrical measurements. Each sample was broken off carefully, in order to avoid unnecessary destruction of the pore space, and the optimum mass of sample to use was determined by trial and error. Enough sample was needed to provide the minimum surface area required for the measurement accuracy of the equipment and the maximum limit on sample quantity was the size of the glass bulb in which the sample is contained. The mass used varied between 2 and 8.5 g, with an average mass of 5.6 g. Samples were dried initially in an oven at 80 °C for 48 h. Then the sample was dried at 150 °C under vacuum by the analysis equipment. This high level of drying was likely to have affected the clay structure but was unavoidable for nitrogen adsorption measurements where a stable high vacuum was required. Even at this temperature a drying time of 8 h was needed to achieve the vacuum required by the equipment. Collapse of the clay structure due to the sample being dry and heated could result in a reduction of surface area from the fully saturated sandstone *in situ*. However, the surface area should still give some guide as to the quantity of pore-lining material. The surface area was calculated using a five-point BET method. The pore surface-area-to-volume ratio (S_{POR}) (Sen *et al.* 1990; Börner *et al.* 1996) is given by

$$S_{POR} = \left[\frac{1-\phi}{\phi}\right] S_m d_m \qquad (7)$$

where d_m is the matrix density in g cm^{-3}, S_m the specific surface area in m^2 g^{-1} and S_{POR} is in units of μm^{-1}.

Mercury injection capillary pressure (MICP)

Background. Mercury injection porosimetry is used to measure the size of pores and the distribution of different pore sizes in a material (Lowell & Shields 1991). A sample of the material is first evacuated, surrounded by mercury and then subjected to increasing pressure to force the mercury into the sample. With each step increase in pressure, the volume of mercury intruded into the sample is recorded. The greater the pressure, the smaller the pores the mercury will intrude into, enabling a pore-size distribution to be determined. In geological studies the technique is often referred to as mercury injection capillary pressure (MICP).

In a sandstone the mercury must pass through the interconnecting spaces between the pores (i.e. the pore throats) in order to fill the pores that are shielded by these spaces. Therefore, importantly, MICP actually measures the pressures needed to intrude mercury through the pore throats. The volume intruded will be entirely dependent on the volume of pore space that is accessed through these pore throats. Bloomfield *et al.* (2001) have made measurements on pore-throat size distributions of Permo-Triassic sandstones from the UK and link them closely with the hydraulic permeability of the rock. Assuming cylindrical pores, mercury porosimetry is capable of measuring pore diameters in the range from 0.3 mm to 30 Å, which is equivalent to a pressure range of 3.5 kPa–414 MPa.

Measurement technique. Mercury injection porosimetry was carried out, using the Micromeritics Autopore III mercury injection porosimeter, on samples taken from the end cuts of the cylindrical cores used for the electrical measurements. Care was taken in sampling in order to maintain the integrity of the pore structure of the sandstone. Samples were then dried at 80 °C for 48 h so that the clay structure was altered as little as possible, although the clays would inevitably be partially dehydrated, causing some change in their structure. An optimum sample mass of between 1.7 and 3.1 g was found by trial and error to use the correct volume of mercury for accurate measurement. Pressure was increased in 54 steps from 3.52 kPa to 228 MPa and the pore-throat diameter, D (in m), at each pressure was given by the Washburn equation (Bloomfield *et al.* 2001)

$$D = \frac{\alpha(-4\cos\theta)}{P_c} \qquad (8)$$

where the contact angle θ is taken as 140°, P_c is the capillary pressure (in N m^{-2}) and α is the interfacial tension taken as 0.485 N m^{-1}.

Model fitting. The results of the MICP are plotted as cumulative volume of intruded mercury against pressure or pore-throat size (Fig. 3). The results for our samples are similar to those presented in a recent study of MICP results for 153 samples of UK Permo-Triassic sandstone by Bloomfield *et al.* (2001).

In Figure 3 mercury is the non-wetting-phase liquid and the assumption is made that there will be some residual water left within the mainly evacuated pores. The 'entry pressure' corresponds to the pressure required to invade the largest pores in the sandstone (Bloomfield *et al.* 2001). The 'breakthrough pressure' corresponds to the formation of a continuum of a non-wetting phase through the pore network and the 'dominant intrusion pressure' is the pressure at which there is maximum intrusion of the mercury. These pressures all correspond to equivalent pore-throat sizes, so that, for example, the dominant intrusion pressure is associated with the dominant pore-throat size.

Here we have modelled the pore-throat distribution using a van Genuchten type equation that has been found to fit the results well (van Genuchten 1980; Bloomfield *et al.* 2001). This is particularly useful because the van Genuchten equation is well known in hydrogeology (Fetter 1999) and the parameters calculated from MICP can then be used to estimate other properties such as entry pressure for contaminants (Gooddy *et al.* 2002) and permeability (van Genuchten 1980; Fetter 1999; Kamath 1992). Before fitting the van Genuchten model

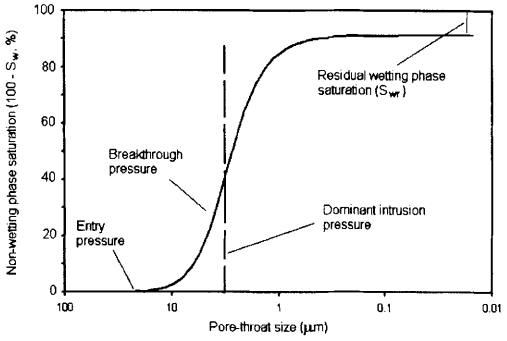

Fig. 3. Pore-throat diameter, from mercury injection capillary pressure curves, against saturation, where mercury is the non-wetting phase.

it was first necessary to modify the MICP data to remove the effect of surface conformance (Bloomfield *et al.* 2001), which is the lowest pressure required to cause the mercury to take on the shape of the rough surface of the sample. This value is subtracted from the subsequent measurements. The van Genuchten model (Bloomfield *et al.* 2001) is given by

$$P_c = P_0\left(S_e^{-1/m_{VG}} - 1\right)^{1-m_{VG}} \quad (9)$$

where P_c is the capillary pressure and P_0 is a characteristic capillary pressure for the medium; Bloomfield *et al.* (2001) consider P_0 to be roughly equivalent to the breakthrough pressure. The parameter, m_{VG}, is a pore-size distribution index. S_e is the normalized wetting-fluid saturation also known as the effective saturation (Fetter 1999) and is given by

$$S_e = \frac{S_w - S_r}{S_m - S_r} \quad (10)$$

where S_w is the wetting fluid saturation, S_r is the residual fluid saturation, in this case the residual water saturation, and S_m is the fluid content at natural saturation, which is taken as 0 as the samples have been dried. The three parameters, P_0, m_{VG} and S_r were fitted to the results using a least-squares minimization with the standard settings for the Solver routine in Microsoft Excel. The breakthrough pore-throat size (D_{P0}) is given by the Washburn equation (equation 8) from the value of P_0.

Three examples of measured MICP curves are given in Figure 4 along with the van Genuchten fits to these data. It is seen that the van Genuchten parameters provide acceptable models for the curves. The most useful parameters are the breakthrough pore-throat sizes (D_{P0}) and m_{VG}. A small value of m_{VG} indicates a greater spread in the distribution of pore-throat sizes. The dominant intrusion occurs at the pressure at which the rate of mercury entering the sample is highest. This is generally close to P_0 and can be calculated by solving,

$$\frac{d^2P_c}{dS_w^2} = 0 \quad (11)$$

to find the dominant intrusion pressure and then from this the dominant pore-throat diameter ($D_{dominant}$) can be calculated from the Washburn equation (equation 8).

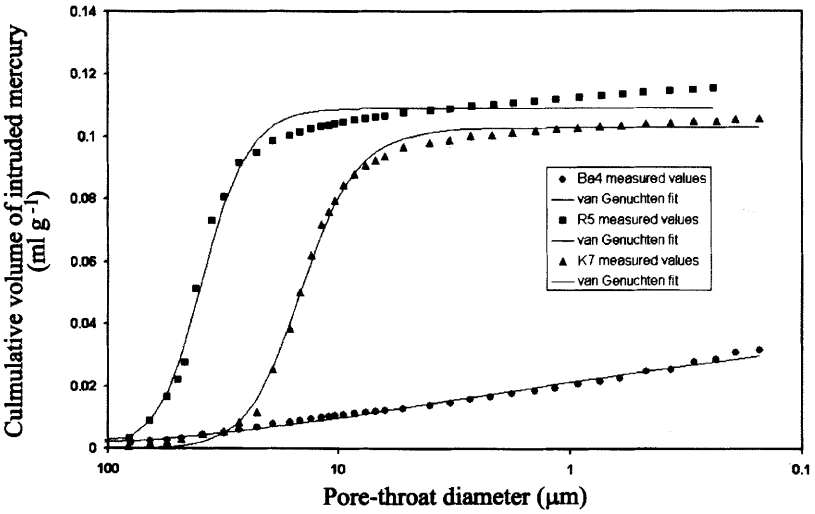

Fig. 4. Mercury injection curves with van Genuchten model parameter fitting (see Table 2 for parameters).

Results

Sandstone properties

The effective porosity, Q_v, S_{POR}, and the van Genuchten parameters for the 28 samples studied are summarized in Table 3 and Figure 5. Porosity generally varies between 15 and 30%, with a mean of 23.6%, which is close to the results of a study of more than 10 000 samples of UK Permo-Triassic sandstone carried out by Allen *et al.* (1997), who measured a mean porosity of 23.8%. Q_v varies between 0.05 and 5.0 meq ml^{-1}, and has a logarithmic distribution as shown in Figure 5B. Pore surface area, S_{POR}, is also best shown as a logarithmic distribution (Fig. 5C), with values varying over two orders of magnitude, from 1 to 100 μm^{-1}. The range of dominant pore-throat size, $D_{dominant}$ is shown in Figure 5D to vary from 5 to 50 μm. Samples Ba4 and Ba21 are notable amongst the Birmingham samples for their relatively low porosity and high Q_v, and Ba4 for its high S_{POR}. Both samples have a low van Genuchten distribution index m_{VG} and, because of the wide distribution of the pore-throat sizes in these two samples, it was not possible to give a dominant pore-throat size. Sample Ba4 contains a significant amount of clay-grade material while sample Ba21 is very fine grained, both reasons for high Q_v and high S_{POR} values. The aeolian samples, K9 and K10, both have relatively low porosities and this is likely to be due to the presence of the pore-filling quartz overgrowths that often surround the grains, quartz having a much lower surface area than clay.

The electrical parameters from the generalized Cole–Cole fitting are summarized in Table 2 and Figure 6. The low-frequency resistivity ($\rho_{5\,mHz}$) ranges over an order of magnitude from 30 to 220 Ωm (Fig. 6A). The normalized chargeability distribution is shown in Figure 6B and the relaxation time distribution in Figure 6C. There is a wide range of relaxation times in these samples, with most falling between 0.74 and 50 s, sample Ba12 is exceptional with a relaxation time of over 300 s.

Correlations

The main aim of this study is the investigation and determination of useful relationships between the frequency-dependent electrical parameters and other important parameters such as porosity, Q_v, S_{POR} and pore-throat size.

The most widely used model for representing the relationship between resistivity and porosity of fully saturated sandstones is probably the following derived by Archie (1942) for a clean sandstone containing no electrically conductive solid material

$$\rho_o/\rho_w = F = a/\phi^m \qquad (12)$$

where F is the formation factor, ρ_o is bulk resistivity, ρ_w the pore-water resistivity, ϕ is the fractional porosity, and a and m are formation constants. The coefficient a is related to

Table 3. *Porosity, cation-exchange capacity, pore surface area and van Genuchten parameters for Permo-Triassic sandstone samples*

Sample	Porosity (%)	Q_v (meq ml^{-1})	S_{POR} (μm^{-1})	van Genuchten parameters from MICP		
				m_{VG}	D_{PO} (μm)	$D_{dominant}$ (μm)
Ba4	12.4	3.60	93.98	0.42	39	
Ba10	28.7	0.32	7.11	0.83	40	36
Ba11	24.8	1.06	15.35	0.78	46	39
Ba12	22.7	0.89	13.81	0.78	56	47
Ba18	21.3	0.87	73.92	0.67	18	12
Ba21	18.8	1.42		0.43	3.1	
Ba23	25.2	1.12	14.95			
Ba31	26.6	0.30	9.65	0.86	34	32
Ba33	27.8	0.70	11.98			
Ba34A	26.9	0.29	25.13	0.83	23	21
Ba34B	26.5	0.30	25.65	0.83	23	21
Ba37	27.7	0.08	12.10		35	33
Ba40	23.4	0.54	58.64	0.80	9.9	8.6
Ba42	27.8	0.80		0.88	43	41
C7	25.8		17.30	0.81	30	27
C8	26.0			0.83	16	15
K7	26.4	0.10	18.77	0.78	16	14
K9	16.3		1.70	0.79	29	25
K10	16.1			0.79	39	33
R5	24.9		11.35	0.82	42	38
R7	23.3			0.77	45	37
R16	24.1	0.15		0.76	24	20
R18	23.6			0.82	34	30
Sa7	27.3	0.67	39.10	0.76	12	9.5
Sb3	31.9	0.29	14.26	0.75	40	32
SH4	15.0			0.75	41	33
W2	20.3		2.71			
W9	19.5	0.06		0.74	27	21
Max.	31.9	3.60	93.98	0.88	56	47
Min.	12.4	0.06	1.70	0.42	3.1	8.6
Mean	23.6	0.71	26	0.76	31	27
SD	4.6	0.80	25	0.11	13	11

tortuosity and is often given the value 1, while m may take values between 1.2 and 4.0 (Winsauer *et al.* 1952; Mendelson & Cohen 1982).

It was recognized early on that departures from this relationship occur when the rock matrix includes minerals that provide additional conductive paths (Waxman & Smits 1968; Barker & Worthington 1973) and associated polarization effects. The presence of polarization effects in shaly sandstone has led to the development of complex resistivity survey and logging techniques. Low-frequency SIP techniques have been carried out in the mHz–kHz range and various studies (Vinegar & Waxman 1984; Börner & Schön 1991) have attempted to define the parameter relationships, but these studies were made on sandstones that had no significant variation in phase angle with frequency. This is not the case for the majority of Permo-Triassic sandstones from the UK. Here we outline the correlations found from our studies.

Chargeability. Our measurements show only a very weak correlation of polarization magnitude, or normalized chargeability, m_n, with Q_v (Fig. 7) and it would be meaningless to try to fit a trend to these data. This contradicts the results of Vinegar & Waxman (1984), who found a correlation between the quadrature conductivity σ'', one measure of polarization magnitude, with Q_v, and Börner *et al.* (1996) who found an approximate correlation between σ'' and CEC.

The correlation between m_n and S_{POR} (Fig. 8) is much stronger and fitting the data with a power trend, using a least-squares regression, gives

$$S_{POR} = a(m_n)^b \quad (13)$$

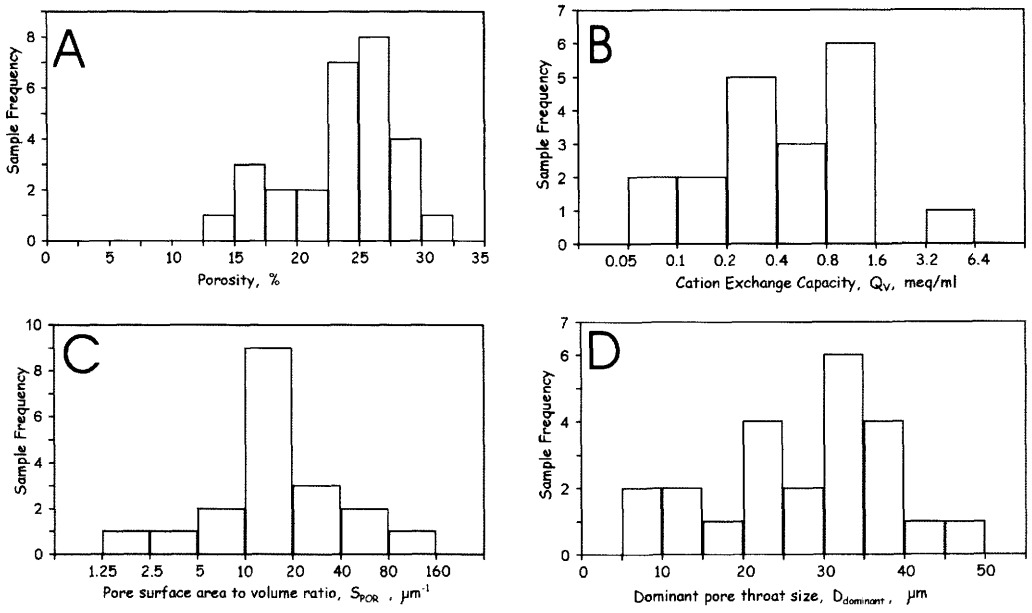

Fig. 5. Histograms of sandstone properties. (**A**) Effective porosity. (**B**) Cation-exchange capacity, Q_v. (**C**) S_{POR} from nitrogen adsorption BET measurement. (**D**) Dominant pore-throat size from mercury injection.

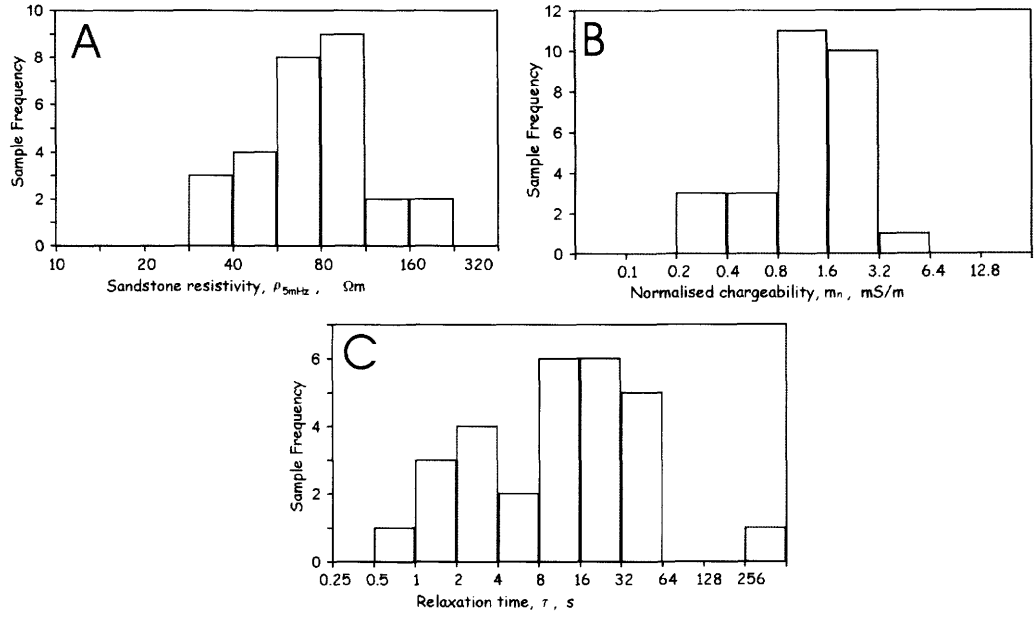

Fig. 6. Histograms of the electrical properties. (**A**) Resistivity at 5 mHz. (**B**) Chargeability from the generalized Cole–Cole model, normalized by the low-frequency resistivity (equation 5). (**C**) Relaxation time from the generalized Cole–Cole model.

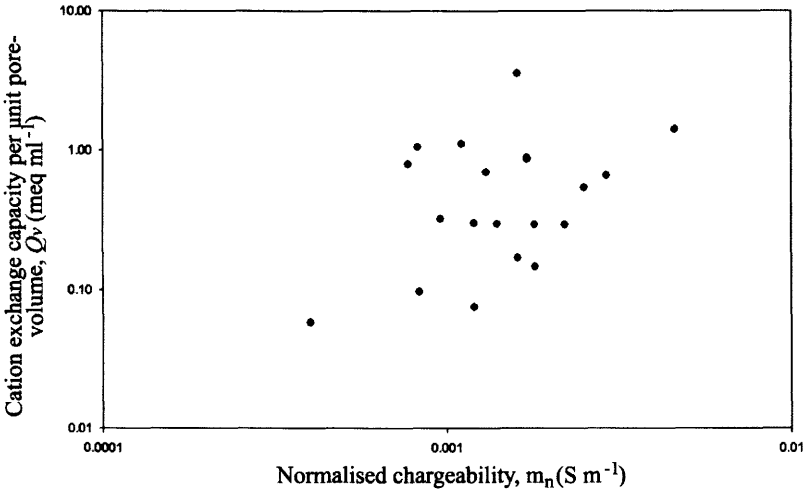

Fig. 7. Comparison of normalized chargeability from the generalized Cole–Cole fit with the cation-exchange capacity to pore volume ratio.

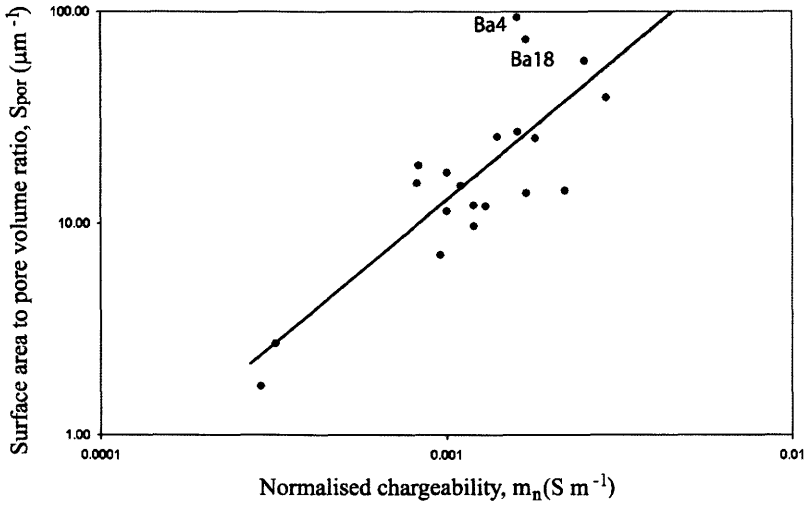

Fig. 8. Comparison of normalized chargeability from the generalized Cole–Cole fit with the surface area to pore volume ratio, calculated using the BET nitrogen adsorption method.

with a correlation coefficient (R^2) of 0.66, where a = 154 000 and b = 1.36. The two samples that fall away from the trend (Ba4 and Ba18) have the two highest S_{POR} values and also have a considerable amount of fine and clay-grade material that is not evenly distributed across the grain surface of the sample. Because of this uneven distribution of surface area, these samples can be removed from the trend to give an improved correlation coefficient of 0.76 with a = 54 400 and b = 1.23. The correlation is very similar to that demonstrated by Börner *et al.* (1996) for their σ''_n parameter which is calculated using their constant phase angle model. However, the results on the samples Ba4 and Ba18 suggest that this nearly linear trend is probably only applicable to homogeneous sandstones with an even distribution of clay or oxides covering the grain surface. The results of Börner *et al.* (1996) and the results shown here suggest that these relationships are only good for an order of magnitude estimate of S_{POR} which could then be used to give permeability estimates by a Kozeny–Carmen type relationship

(Börner *et al.* 1996). Although further ambiguities may make the results inaccurate, modified versions of this permeability estimation method have shown some reasonable results for unconsolidated sediments (Slater & Lesmes 2002). However, the Kozeny–Carmen type permeability model is based on samples with low surface area having higher permeability, and this relationship is likely to be inappropriate for these samples because the presence of the quartz overgrowths (e.g. samples K9 and K10) is likely to significantly lower the permeability as well as the surface area.

Relaxation time. The correlation between pore-throat size and relaxation time is shown in Figures 9 and 10 for all samples for which both the van Genuchten and generalized Cole–Cole parameters were determined, except sample Ba18 which has a strong clay banding and is highly inhomogeneous. The error in the τ calculation is the most significant and error bars have been included for all samples (Fig. 9). The samples with an error in τ of less than 50% have been fitted with logarithmic trends, using a least-squares regression. The correlation between D_{P0} and τ (solid line in Fig. 9) is given by

$$D_{P0} = 8.04 \ln \tau + 14.0 \quad (14)$$

with a correlation coefficient of 0.75, where D_{P0} is in μm and τ is in s. The correlation between $D_{dominant}$ and τ (solid line in Fig. 10) is given by

$$D_{dominant} = 6.87 \ln \tau + 12.4 \quad (15)$$

with a correlation coefficient of 0.73, where $D_{dominant}$ is in μm and τ is in s. This correlation between $D_{dominant}$ and τ is similar to the results given by Scott & Barker (2003) where the dominant pore-throat diameter, $D_{dominant}$, is shown to correlate with the phase peak frequency, f_{peak}, based on a smaller set of samples. Converting the dominant pore-throat value to μm the fit shown by Scott & Barker (2003) is given by

$$D_{dominant} = 5.9 \ln \tau + 27 \quad (16)$$

where the relationship between relaxation time and peak frequency is given by

$$\tau = \frac{1}{2\pi f_{peak}}. \quad (17)$$

The model fitting may be more practical because D_{P0} is easily calculated and is very close in value to $D_{dominant}$, and the discrete increases in mercury pressure make accurate picking of $D_{dominant}$ difficult. It can also be difficult to pick f_{peak} due to the use of discrete frequencies. From the generalized Cole–Cole model τ has been shown to have a potentially large error, particularly when there is a wide spread of the phase peak region, and fitting of this model gives an estimate of the potential range of τ. Therefore the model fitting of the van Genuchten and generalized Cole–Cole parameters, along with an appropriate error analysis, can give more meaningful results on a wider range of samples.

Distribution. Owing to the correlation between D_{P0} and τ, shown above, it should be expected that there will be some correlation between the distribution parameters m_{VG}, c and k. Samples Ba4 and Ba21 both have a widely spread pore-throat size distribution and hence have the lowest values of m_{VG}. They also have extremely low values of c and k, and no clear peak relaxation time. However, samples with low chargeability also have widely spread relaxation times and hence low values of c and k, a notable example being sample W2. This implies that the correlation between the pore-throat size distribution and the spread of the electrical spectra is also dependent on the magnitude of the polarization. Therefore any correlation between the parameters m_{VG}, c and k should either be done only on samples with a high enough polarization or should take into account the magnitude of the polarization. It would be necessary to have a larger data set in order to examine this possible correlation.

Discussion

General findings

The results presented above reinforce the idea of Börner & Schön (1991) that the magnitude of the low-frequency polarization in sandstones is dependent on the pore surface area. However, this is only true for the homogeneous samples that have an even distribution of clays or oxyhydroxides around the grains giving an even distribution of surface area throughout the sandstone. Samples with quartz overgrowths or calcite cement, the aeolian samples from Kirkham and the samples from Winterbourne Kingston have an increasingly lower pore surface area giving rise to a significantly lower polarization than the other samples. Pore surface area is not only important for possible permeability calculation (Börner *et al.* 1996) but also in estimating the potential sorbtion of any contaminants passing through the rock.

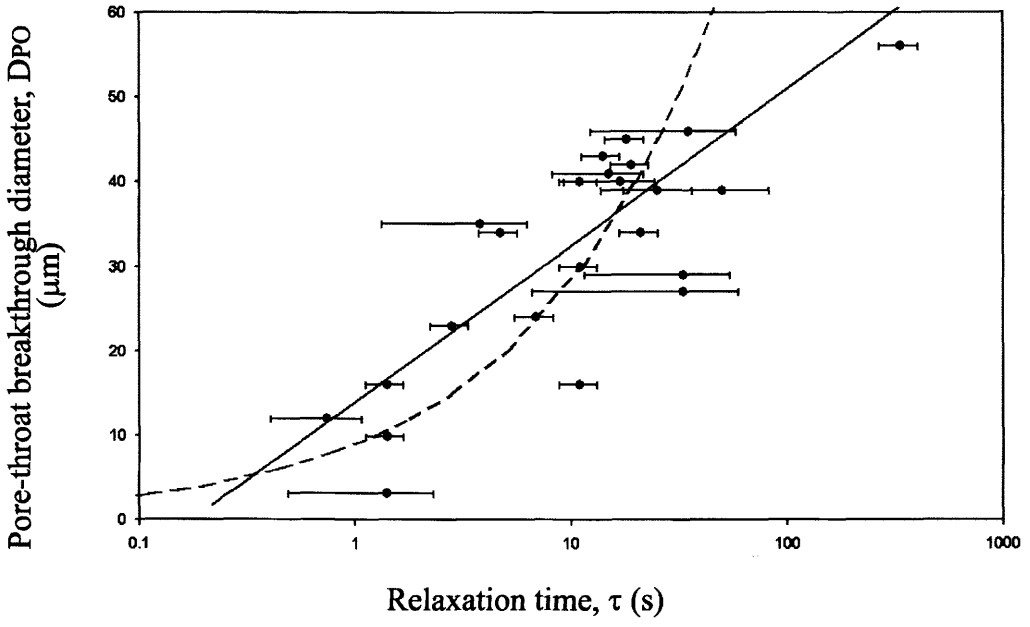

Fig. 9. Comparison of relaxation time from the generalized Cole–Cole fit with the breakthrough pore-throat diameter, from van Genuchten fitting of mercury injection curves. The solid line shows a logarithmic trend fitted to samples with a τ error $\leq 50\%$. The dashed line shows the best fit of the spherical colloid relaxation model (equation 18) using the pore-throat diameter.

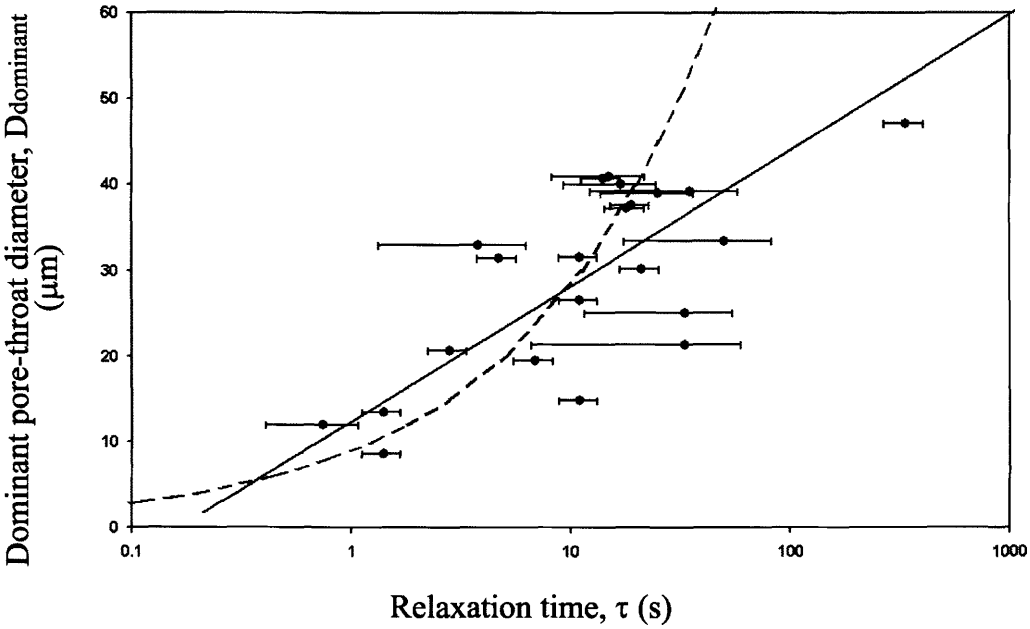

Fig. 10. Comparison of relaxation time from the generalized Cole–Cole fit with the dominant pore-throat diameter, calculated from van Genuchten fitting of mercury injection curves. The solid line shows a logarithmic trend fitted to the results. The dashed line shows the best fit of the spherical colloid relaxation model (equation 18) using the pore-throat diameter.

As the magnitude of the polarization is a measure of the quantity of ions associated with the pore surface, it is expected to show a stronger correlation with Q_v than does the pore surface area. However, this was not the case here.

There is a good correlation between relaxation time and pore-throat size, although it is not possible to be certain from these results exactly what length scale in the sandstone gives rise to the observed relaxation times. Possible relaxation time length scales in the sandstone are pore-throat diameter, pore diameter, length between pore throats or length of pore throat, these in combination with the varying shapes of the pores and pore throats mean that a much higher level of measurement of the pore geometry would be needed to examine which length scale or combination of length scales was the most important. However, the correlation between pore-throat diameter and relaxation time is strong enough to be able to make a calculation of the pore-throat size from the electrical measurements and to use this to estimate the permeability of the sandstone or the entry pressure needed for non-aqueous contaminants or even commercial hydrocarbons.

The amount of information contained in the electrical spectra of a sandstone means that not only can hydrogeologically important parameters be derived but also that the electrical spectra may be an effective way of fingerprinting a particular lithology. This could prove useful in correlating between boreholes.

Modelling

Relaxation models. Although it has been found that the pore geometry is an important factor in the low-frequency relaxation observed in sandstones, there is still some debate as to which ions are the most significant and what is the exact relaxation mechanism. It is generally accepted that the polarization and corresponding low-frequency relaxation in non-metallically mineralized sandstones is caused by ion diffusion in or around the electrochemical double layer (EDL) (Nettelblad & Niklasson 1997; Chelidze & Gueguen 1999; Lesmes & Morgan 2001). The EDL is formed when a liquid containing ions is in contact with the solid rock matrix. Then the rock surface tends to have an associated negative charge. This surface negative charge attracts cations to it that form an EDL. The Stern model of the EDL (Reppert *et al.* 2001) consists of a layer (the Stern layer) where ions are relatively immobile and held rigidly by electrostatic forces. Beyond this there is a diffuse layer that extends into the solution (the Gouy–Chapman diffuse layer).

Ions in and around the EDL are less mobile than those in the pore fluid and the excess of cations in the EDL along with different layer mobilities causes relative movement of charge resulting in polarization. The main contributions to the in-phase and quadrature low-frequency electrical conduction are generally considered to be the movement of ions in the Stern and the diffuse layers. There is also some suggestion that a membrane type polarization occurs, where in zones such as pore throats the cations in the pore fluid are more mobile than the anions due to the blocking effect of the EDL. This type of model was proposed by Marshal & Madden (1959) and has been used recently by Titov *et al.* (2002); in this case both the length of the pore and the length of the pore throat could make a significant contribution to the electrical relaxation. However, it is generally accepted that the excess, in-phase conductivity observed in shaly sandstone is the result of movement of cations in the EDL. Revil & Glover (1998) and Revil (1999) claim that most of this excess conductivity is due to cations moving in the Stern layer. Ions in the Stern layer are free to 'site hop' between exchange sites along the surface, and monovalent ions are generally only weakly bound and free to move tangentially along the grain surface. This excess movement of cations, either in the Stern or diffuse layers, is also most likely to be the cause of the observed polarization and the observed quadrature conductivity. Lesmes & Morgan (2001) suggest that movement of cations in the Stern layer is important in the polarization of sandstone. Relaxation models for these surface type EDL relaxations have generally been developed on colloidal particles. The simplest models of this type in general use are for relaxation around a sphere (Schwarz 1962; Dukhin & Shilov 1974; Fixman 1980). The relaxation time for ions in the Stern layer from these models is given by

$$\tau_s = \frac{R^2}{2D_s} \tag{18}$$

where τ_s is the relaxation time, R is the radius of the sphere and D_s is the diffusion coefficient of the ions in the Stern layer. Correspondingly, a similar equation can apply to the diffuse layer, where τ_d and D_d are the relaxation time and diffusion coefficient, respectively, for ions in the diffuse layer.

Ion mobility. The ion diffusion coefficient is extremely important as this controls the

relaxation time as well as the length scale involved. Lesmes & Morgan (2001) use a bulk pore-fluid diffusion coefficient of $D_{bulk} = 2 \times 10^{-9}$ m^2 s^{-1} for KCl and state that in general $D_s < D_d < D_{bulk}$, where D_{bulk} is the diffusion coefficient away from the EDL. They state that a diffusion coefficient, $D = 0.11\ D_{bulk}$ best fits their data and so assume this is the diffusion coefficient in the EDL; for this they use the grain radius as the relaxation length, assuming that the sand grains behave like spherical colloidal particles, even though the grains are often tightly packed. An equivalent model is applied to the pores, with the pore size being assumed to be approximately the same as the grain size.

The absolute mobility, μ, of an ion is related to the diffusion coefficient by the Einstein–Smoluchowski relation:

$$D = \frac{\mu k T}{e} \tag{19}$$

where k is Boltzman's constant, T is the absolute temperature and e is the charge of an electron. Revil (1999) gives some typical mobility values for monovalent ions, quoting a dilute solution mobility for Na^+ at 25 °C of 5.19×10^{-8} m^2 s^{-1} V^{-1}. Revil (1999), using the results of Raythatha & Sen (1986) on clay suspensions, estimates a Stern layer mobility for Na^+ at 25 °C of 5.14×10^{-9} m^2 s^{-1} V^{-1} claiming this to be independent of clay mineral type. Calculation of the diffusion coefficient for Na^+ from the results of Revil (1999) and equation 19 gives a bulk value, D_{bulk}, of 1.31×10^{-9} m^2 s^{-1} and a surface diffusion value, D_s, of 1.31×10^{-10} m^2 s^{-1}. The surface ion mobility, μ_s, and hence the surface diffusion, D_s, can be estimated from the excess in-phase conductivity, σ_s, and Q_v (Revil 1999) using

$$\mu_s \approx \frac{3}{2}\left(\frac{1-\phi}{\phi}\right)\frac{\sigma_s}{Q_v} \tag{20}$$

where σ_s is calculated from multiple salinity measurements. Using the results of Taylor & Barker (2006) on UK Permo-Triassic sandstone gives a $D_s = 6.58 \times 10^{-11} \pm 2.4 \times 10^{-11}$ m^2 s^{-1} for Na^+, which is slightly lower than the values given above. The measurements in this study use a synthetic groundwater containing a concentration ratio of approximately 2:1:1 for Ca^{2+}:Na^+:Mg^{2+}. Calcium and magnesium ions are less mobile in bulk solution and being bivalent would be expected to be more strongly bonded in the EDL, further reducing their mobility.

Application to experimental results. The results of Börner *et al.* (1993) and Scott & Barker (2002) show that Na^+ gives a higher magnitude polarization than Ca^{2+} and Mg^{2+} so it is likely to have a major contribution to the combined relaxation effect, although Ca^{2+} and Mg^{2+} are preferentially bonded to the exchange sites at the mineral surface making the effects on the double layer complicated. Using a simple spherical grain size relaxation model, the observed relaxation times, in the range of 1–100 s in this study and the range of sandstone grain diameters of 0.1–1 mm (fine–coarse), would require a D_s of 1.25×10^{-9} m^2 s^{-1}, which is equivalent to the bulk diffusion coefficient. This shows that the relaxation length scale is not the grain diameter if this is a correct model to use. The dashed line in Figures 9 and 10 is the best fit of the spherical colloid relaxation model (equation 18) to the pore-throat size and this uses a D_s value of 1×10^{-11} m^2 s^{-1}, which is slower than the diffusion coefficient suggested by the results of Taylor & Barker (2006). Simple relaxation models can only provide estimates, and the uncertainty in relaxation processes and diffusion coefficients makes length scale estimates inaccurate. However, the correlation with pore-throat size in Figures 9 and 10 and equations (14) and (15) are extremely good and indicate the possibility of this being the most important length scale. For example, sample Ba12 does not have a larger grain size than some of the other samples but its relaxation time is much greater. The sample also has the largest pore-throat size, which suggests that the length scale may be related to pore-throat size or possibly pore size, but *not* the grain size. Pore throats are not always simple spheres and the length of the pore throats may also be extremely important; this has already been suggested by Titov *et al.* (2002). A lot of further work is necessary including image analysis for grain-size and pore-size distributions in order to make more informed conclusions.

Another important factor that is often ignored is that the strength of the electrical relaxation will also be affected by the dimensions of the pore or pore throat. Low-frequency conduction is mainly through the bulk pore fluid and in the main pore volume there is a lower surface area to volume ratio than in the pore-throats. With the greater in-phase conduction through this fluid it can be seen from equation 1 that this would reduce the phase angle measured. Therefore the surface conduction in pore throats would be expected to be far more significant than that in the main pore space. It is important to note that the basic relaxation

models cannot be applied directly to sandstones because the dimensions and shape of pores and pore throats will vary significantly. Also the pore-throat diameter calculated from mercury injection will also not be accurate because it is based on a simple cylindrical model. Therefore the correlations observed here are extremely good considering the various ambiguities and inaccuracies involved.

Conclusions

The low-frequency electrical spectra of Permo-Triassic sandstone from the UK are often characterized by a relaxation phenomenon that can be seen clearly as a negative peak in the phase spectra. The relaxation peaks when present are usually asymmetric and can be modelled by a generalized Cole–Cole equation (Klein & Sill 1982; Dias 2000). This model gives five parameters that describe the spectra well over at least three decades of frequency, and sometimes as many as all five decades of frequency between 0.001 and 100 Hz. The parameters all have electrical significance and correlate well with other hydrogeologically important parameters obtained from the techniques of MICP and nitrogen adsorption. Of particular importance is that the relaxation time, τ, is strongly related to the dominant pore-throat size. This could have many hydrogeologically important, uses including permeability estimation based on van Genuchten models (Kamath 1992). A normalized version of the chargeability appears to be related to the surface conductivity and this gives the possibility of estimating the pore surface area to volume ratio, a value that is important both in permeability estimation and in sorption estimation with relation to contaminant transport. There is a correlation between the spread of the relaxation distribution and the spread of the pore-throat distribution, although this is weak due to the interaction of other parameters such as chargeability. Finally, the electrical spectra for shaly sandstone contain so much information that they could potentially provide an effective lithological fingerprint. There is a need for many more extensive studies on sandstones using both real and artificial samples, and development of the associated theory of the electrical relaxation processes taking place. The potential uses of electrical spectroscopy in hydrogeology and many other fields including geology and petroleum petrophysics are only now becoming apparent, and further advances are certain.

The authors wish to thank P. Atkins for assistance with electrical measurements and H. Mills for assistance in nitrogen adsorption and mercury injection measurements. Our thanks also to the British Geological Survey, Wallingford for providing sandstone samples for this study. A number of people have assisted with the laboratory work and we would like to thank P. Hands, R. Livesey and J. Harris. Finally, we would like to acknowledge J. Tellam and S. Taylor for their helpful discussions.

References

ALLEN, D.J., BREWERTON, L.J. *ET AL.* 1997. *The Physical Properties of Major Aquifers in England and Wales*. British Geological Survey, Technical Report, **WD/97/34**. Environment Agency R&D Report Publication, **8**.

ARCHIE, G.E. 1942. The electrical resistivity log as an aid in determining some reservoir characteristics. *Transactions of the American Institute of Mining, Metallurgical and Petroleum Engineers*, **146**, 54–62.

BARKER, R.D. & WORTHINGTON, P.F. 1973. Some hydrogeophysical properties of the Bunter sandstone of northwest England. *Geoexploration*, **11**, 151–170.

BLOOMFIELD, J.P., GOODDY, D.C., BRIGHT, M.I. & WILLIAMS, P.J. 2001. Pore-throat size distributions in Permo-Triassic sandstones from the United Kingdom and some implications for contaminant hydrogeology. *Hydrogeology Journal*, **9**, 219–230.

BÖRNER, F.D. & SCHÖN, J.H. 1991. A relation between the quadrature component of electrical conductivity and the specific surface area of sedimentary rocks. *The Log Analyst*, **32**, 612–613.

BÖRNER, F.D., GRUHNE, M. & SCHÖN, J.H. 1993. Contamination indications derived from electrical properties in the low-frequency range. *Geophysical Prospecting*, **41**, 83–98.

BÖRNER, F.D., SCHOPPER, J.R. & WELLER, A. 1996. Evaluation of transport and storage properties in the soil and groundwater zone from induced polarization measurements. *Geophysical Prospecting*, **44**, 583–601.

CHELIDZE, T.L. & GUEGUEN, Y. 1999. Electrical spectroscopy of porous rocks: a review – I. Theoretical models. *Geophysical Journal International*, **137**, 1–15.

DIAS, C.A. 2000. Developments in a model to describe low-frequency electrical polarisation of rocks. *Geophysics*, **65**, 437–451.

DUKHIN, S.S. & SHILOV, V.N. 1974. *Dielectric Phenomena and the Double Layer in Disperse Systems and Polyelectrolytes*. Wiley, New York.

FETTER, C.W. 1999. *Contaminant Hydrogeology*, 2nd edn. Prentice-Hall, Upper Saddle River, NJ.

FIXMAN, M. 1980. Charged macromolecules in external fields, I, the sphere. *Journal of Chemical Physics*, **72**, 5177–5186.

GOODDY, D.C., BLOOMFIELD, J.P., HAROLD, G. & LEHARNE, S.A. 2002. Towards a better understanding of trichloroethene entry pressure in the matrix of Permo-Triassic sandstones. *Journal of Contaminant Hydrology*, **59**, 247–265.

JONSCHER, A.K. 1983. *Dielectric Relaxation in Solids*. Chelsea Dielectrics Press, London.

JONSCHER, A.K. 1996. *Universal Relaxation Law*. Chelsea Dielectrics Press, London.

KAMATH, J. 1992. Evaluation of accuracy of estimating air permeability from mercury injection data. *SPE Formation Evaluation*, **4**, 304–310.

KLEIN, J.D. & SILL, W.R. 1982. Electrical properties of artificial clay-bearing sandstone. *Geophysics*, **47**, 1593–1605.

KREMER, F. 2002. Dielectric spectroscopy – yesterday, today and tomorrow. *Journal of Non-crystaline Solids*, **305**, 1–9.

LESMES, D.P. & FRYE, K.M. 2001. Influence of pore fluid chemistry on the complex conductivity and induced polarization responses of Berea sandstone. *Journal of Geophysical Research*, **106**, 4079–4090.

LESMES, D.P. & MORGAN, F.D. 2001. Dielectric spectroscopy of sedimentary rocks. *Journal of Geophysical Research*, **106**, 13 329–13 346.

LOWELL, S. & SHIELDS, J.E. 1991. *Powder Surface Area and Porosity*, 3rd edn. Chapman & Hall, London.

MARSHALL, D.J. & MADDEN, T.R. 1959. Induced polarization, a study of its causes. *Geophysics*, **24**, 790–816.

MENDELSON, K.S. & COHEN, M.H. 1982. The effect of grain anisotropy on the electrical properties of sedimentary rocks. *Geophysics*, **47**, 257–263.

MITCHENER, R.G.R. 2003. *Hydraulic and chemical property correlations of the Triassic Sandstone of Birmingham*. PhD thesis, University of Birmingham.

NETTELBLAD, B. & NIKLASSON, G.A. 1997. Dielectric relaxations in liquid-impregnated porous solids. *Journal of Materials Science*, **32**, 3783–3800.

OLHOEFT, G.R. 1985. Low-frequency electrical properties. *Geophysics*, **50**, 2492–2503.

PELTON, W.H., WARD, S.H., HALLOF, P.G., SILL, W.R. & NELSON, P.H. 1978. Mineral discrimination and removal of inductive coupling with multifrequency IP. *Geophysics*, **43**, 588–609.

RAYTHATHA, R. & SEN, P.N. 1986. Dielectric-properties of clay suspensions in MHz to GHz range. *Journal of Colloid and Interface Science*, **109**, 301–309.

REPPERT, P.M., MORGAN, F.D., LESMES, D.P. & JOUNIAUX, L. 2001. Frequency-dependent streaming potentials. *Journal of Colloid and Interface Science*, **234**, 194–203.

REVIL, A. 1999. Ionic diffusivity, electrical conductivity, membrane and thermoelectric potentials in colloids and granular porous media: A unified model. *Journal of Colloid and Interface Science*, **212**, 503–522.

REVIL, A. & GLOVER, P.W.J. 1998. Nature of surface electrical conductivity in natural sands, sandstones and clays. *Geophysical Research Letters*, **25**, 691–694.

SCHWARZ, G. 1962. A theory for the low-frequency dielectric dispersion of colloidal particles in electrolyte solution. *Journal of Physical Chemistry*, **66**, 2636–2642.

SCOTT, J. & BARKER, R. 2002. The spectral induced polarisation response of Triassic sandstone from the United Kingdom. *In: Proceedings of the 8th Meeting of the Environmental and Engineering Geophysical Society – European Section, Aviero, EEGS*, 363–366.

SCOTT, J.B.T. & BARKER, R.D. 2003. Determining pore-throat size in Permo-Triassic sandstones from low-frequency electrical spectroscopy. *Geophysical Research Letters*, **30**, 1450.

SCOTT, J., SCHLEIFER, N., WELLER, A. & BARKER, R. 2003. The spectral induced polarisation of groundwater saturated sandstones. *In: Proceedings of the 9th European Meeting of Environmental and Engineering Geophysics, Prague, EEGS*, 265–268.

SEIGEL, H.O. 1959. A theory for induced polarization effects (for step excitation function). *In*: WAIT, J.R. (ed.) *Overvoltage Research and Geophysical Applications*. Pergamon Press, New York, 4–21.

SEN, P.N., STRALEY, C., KENYON, W.E. & WHITTINGHAM, M.S. 1990. Surface-to-volume ratio, charge density, nuclear magnetic relaxation, and permeability in clay-bearing sandstones. *Geophysics*, **55**, 61–69.

SLATER, L. & LESMES, D.P. 2002. Electrical-hydraulic relationships observed for unconsolidated sediments. *Water Resources Research*, **38**, 1213.

TAYLOR, S. & BARKER, R. 2002. Resistivity of partially saturated Triassic sandstone. *Geophysical Prospecting*, **50**, 603–613.

TAYLOR, S. & BARKER, R.D. 2006. Modelling the DC electrical response of fully and partially saturated Permo-Triassic sandstone. *Geophysical Prospecting* (in press).

TITOV, K., KOMAROV, V., TARASOV, V. & LEVITSKI, A. 2002. Theoretical and experimental study of time domain-induced polarization in water-saturated sands. *Journal of Applied Geophysics*, **50**, 417–433.

VAN GENUCHTEN, M.TH. 1980. A closed-form equation for predicting the hydraulic conductivity of unsaturated soils. *Soil Science Society of America Journal*, **44**, 892–898.

VAN VOORHIS, G.D., NELSON, P.H. & DRAKE, T.L. 1973. Complex resistivity spectra of porphyry copper mineralization. *Geophysics*, **38**, 49–60.

VINEGAR, H.J. & WAXMAN, M.H. 1984. Induced polarisation of shaly sands. *Geophysics*, **49**, 1267–1287.

WAXMAN, M.H. & SMITS, L.J.M. 1968. Electrical conductivities in oil-bearing shaly sands. *Society of Petroleum Engineers Journal*, **243**, 107–122.

WINSAUER, W.O., SHEARIN, H.M., JR., MASSON, P.H. & WILLIAMS, M. 1952. Resistivity of brine-saturated sands in relation to pore-geometry. *AAPG Bulletin*, **36**, 253–277.

WORTHINGTON, P.F. 1976. Hydrogeophysical properties of parts of the British Trias. *Geophysical Prospecting*, **24**, 672–695.